JOURNAL OF GUIDANCE, CONTROL, AND DYNAMICS
Vol. 29, No. 6, November–December 2006

Simplified Technique for Modeling Piloted Rotorcraft Operations Near Ships

Ronald A. Hess*
University of California, Davis, Davis, California 95616

DOI: 10.2514/1.18711

A simplified framework for evaluating a rotorcraft control system design in the overall operational context of task, pilot, and environment is provided for flight operations near ships. The approach uses a simplified, closed-form formulation for ship motion, a control algorithmic model of the human pilot, and a simplified technique for modeling atmospheric disturbances. An approach for estimating multiloop handling qualities is presented. The proposed methodology is exercised in an example of a rotorcraft in a station-keeping task near the deck of a high-speed ferry in the presence of significant environmental disturbances in terms of both ship motion and turbulence.

Nomenclature

$[A]$, $[B]$ = matrices describing rotorcraft dynamics
B = ship average breadth, m
B_0 = ship maximum waterline breadth, m
C = command signal in single-axis structural pilot model
C_b = ship block coefficient, B/B_0
F_n = Froude number, $V/\sqrt{gL}$
GM_T = ship transverse metacentric height, m
G_θ = rotorcraft stability augmentation transfer function for pitch loop
$G_{\theta c}$ = rotorcraft command augmentation transfer function for pitch loop
G_ϕ = rotorcraft stability augmentation transfer function for roll loop
$G_{\phi c}$ = rotorcraft command augmentation transfer function for roll loop
G_r = rotorcraft stability augmentation transfer function for yaw-rate loop
H_S = significant wave height, m
h_P = heave motion of ship pad, m
h_S = ship heave motion, m
$K_{\dot{m}}$ = gain in vestibular feedback loop in structural pilot model
K_{δ_A} = conversion factor from rotorcraft swashplate angle to equivalent cockpit controller motion
L = ship length at waterline, m
M = output signal in single-axis structural pilot model
p = rotorcraft roll rate, rad/s
q = rotorcraft pitch rate, rad/s
R_m = rotorcraft main-rotor radius, m
r = rotorcraft yaw rate, rad/s
T = ship mean draught, m
T_N = ship roll time constant, s
T_S = wave mean period, s
T_Z = wave mean up-crossing period, s
U_M = proprioceptive feedback signal in structural pilot model
U_0 = rotorcraft trim airspeed, m/s
u = x body-axis component of rotorcraft velocity perturbation, m/s
V_r = mean wind speed in turbulence model, m/s
v = y body-axis component of rotorcraft velocity perturbation, m/s
w = z body-axis component of rotorcraft velocity perturbation, m/s
wn = white noise with unity covariance
Y_e = visual signal compensation in structural pilot model
Y_{FS} = model of force/feel system dynamics in structural pilot model
Y_{NM} = model of neuromuscular dynamics in structural pilot model
Y_{PF} = proprioceptive feedback compensation in structural pilot model
Yp_h = outer-loop pilot model transfer function for vertical translation control
$Yp_{\dot{h}}$ = overall structural model transfer function for heave-rate control
Yp_x = outer-loop pilot model transfer function for longitudinal translation control
Yp_y = outer-loop pilot model transfer function for lateral translation control
Yp_θ = overall structural model transfer function for pitch control
Yp_ϕ = overall structural model transfer function for roll control
Yp_ψ = overall structural model transfer function for yaw control
y_P = lateral motion of ship landing pad, m
β = wave direction heading angle, rad
δ_A = lateral cyclic input, centimeters of equivalent cockpit controller motion measured at pilot's hand
δ_{Ap} = pilot's lateral cyclic input, centimeters of cockpit controller motion measures at pilot's hand
δ_B = longitudinal cyclic input, centimeters of equivalent cockpit controller motion measured at pilot's hand
δ_{Bp} = pilot's longitudinal cyclic input, centimeters of cockpit controller motion measured at pilot's hand
δ_C = collective input, centimeters of equivalent cockpit controller motion measured at pilot's hand
δ_{Cp} = pilot's collective input, centimeters of cockpit controller motion measured at pilot's hand
δ_P = pedal input, centimeters of equivalent cockpit controller motion measured at pilot's feet
δ_{Pp} = pilot's pedal input, centimeters of cockpit controller motion measured at pilot's foot
θ = rotorcraft pitch attitude, rad
θ_S = ship pitch, rad
μ = percentage critical damping

Presented as Paper 6030 at the AIAA Atmospheric Flight Mechanics Conference and Exhibit, San Francisco, CA, 15–18 August 2005; received 9 July 2005; revision received 20 February 2006; accepted for publication 21 February 2006.

*Professor, Department of Mechanical and Aeronautical Engineering. Associate Fellow AIAA.

σ_w = root mean square value of vertical gust velocity, m/s
τ_0 = time delay in structural pilot model
ϕ = rotorcraft roll attitude, rad
ϕ_S = ship roll, rad
ψ = rotorcraft heading, rad

I. Introduction

AIRCRAFT shipboard operations, whether fixed or rotary wing, represent demanding flight tasks for the pilot and can be potentially hazardous to personnel, both in the cockpit and on the flight deck. Determining the suitability of existing or proposed vehicle flight control system designs for operations near ships is an important, if not critical, design consideration. The availability of simplified approaches for evaluating these designs through analysis and computer simulation would constitute an important tool for the flight control and handling qualities engineer.

High-fidelity modeling of the near-ship environment for aircraft operations is a complex undertaking especially in terms of modeling atmospheric disturbances, for example, [1–7]. The computational requirements associated with such models, however, may inhibit their use as a tool for the flight control or handling qualities engineer. For example, the detailed computational fluid dynamics (CFD) model of the airwake of an amphibious assault ship developed in [6] required 1.8 hours of processor time on 12 parallel processors to compute 1 s of real-time flow data. The computer requirements associated with this turbulence model led to the adoption of a simplified treatment of turbulence in [7], very similar to the approach espoused in the research to be described. Atmospheric turbulence effects will be treated using the approach discussed in [8], with appropriate vehicle scaling treated using the method presented in [9].

The use of simplified approaches for determining ship motion will also be of interest in this study. Reference [10] describes a study wherein a simple ship roll-motion model is used in examining aeroelastic rotorcraft blade dynamics in shipboard engage/disengage sequences. Here, the work of [11] will be used, wherein a semianalytical approach to derive transfer functions for producing wave-induced motions for monohull ships was developed. Reference [11] provides closed-form expressions for ship motion power spectral densities using information restricted to ship length, breadth, draught, block coefficient, speed and heading, and information regarding sea state. The paper is organized as follows: Section II provides a brief summary of extant models of the human pilot. Sections III and IV summarize the methods for generating ship motion and modeling atmospheric turbulence, respectively. Section V provides an example of applying the analysis technique to a hypothetical task involving a rotorcraft attempting fine position tracking near the landing pad of a high-speed ferry. Conclusions are drawn in Sec. VI.

II. Pilot Models

An overview of pilot modeling techniques is best approached by considering the different types of human operator models that have been developed to date.

A. Isomorphic Models

Isomorphic models refer to those models of pilot control behavior in which some effort has been directed toward explicitly modeling the dynamics of the human sensory and control effector systems. Two examples of this type of model are 1) the crossover model, and 2) the structural model.

1. *Crossover Model*

This model, itself, is not an isomorphic model. However, its central importance in manual control theory and its relationship to more advanced models of human control behavior require at least a brief discussion. Basically, the crossover model stipulates the form of the open-loop pilot/vehicle system in so-called single-axis tracking tasks. That is, in the region of the open-loop crossover frequency, the product of the pilot's transfer function and that of the vehicle will resemble an integrator with time delay [12].

2. *Structural Model*

This model offers a simplified structural representation of pilot dynamics in compensatory systems [13]. The model hypothesizes the importance of proprioceptive cues in allowing the human pilot to adopt the necessary equalization to meet the experimentally validated form of the crossover model.

3. *Biophysical Models*

Reference [14] presents a detailed biophysical model of the human pilot, with particular emphasis on the dynamics of the pilot's neuromuscular system. The impetus behind the development of this model was the introduction of fly-by-wire systems in modern aircraft.

4. *Biodynamic Models*

The fact that pilots of modern aircraft can be subjected to accelerating or vibrating environments that may adversely affect their performance has led to the formulation of biodynamic models of human pilot behavior. With these models, one can investigate the effects of an accelerating/vibrating environment on the pilot's control capabilities. An example of one such a model is discussed in [15].

B. Algorithmic Models

Algorithmic models refer to those models of pilot control behavior that are created through the use of synthesis techniques that have been successfully applied to the design of inanimate controllers. Some isomorphism may be retained in the modeling procedure.

1. *Optimal Control Model*

The optimal control model (OCM) of human pilot control behavior is probably the best known of the algorithmic models [16]. The OCM represents the solution to a linear, quadratic, Gaussian (LQG) control problem. The model is particularly attractive because efficient computational tools are available for its implementation, for example, [17]. It was the OCM of the human pilot that was employed in [6,7].

C. Behavioral-Based Models

For lack of a better name, a class of models of human pilot behavior can be identified as behavioral-based models. These models rely upon novel and often detailed representations of human signal processing behavior. Two such approaches are outlined briefly, next.

1. *Fuzzy-Logic Models*

So-called fuzzy-logic models of human pilot behavior have been developed, for example, [18]. Strictly speaking, these models are not control-theoretic in nature, as fuzzy-set theory leads to a description of cause-and-effect relationships that differ considerably from the control-theoretic constructs that have been described to this point. These models have been used to describe such diverse human control activity as helicopter piloting [18] and automobile driving [19].

2. *Neural Net Models*

These models of human pilot behavior rely upon the power of neural nets to accurately describe the nonlinear signal processing behavior of the human. These models are particularly useful in mapping pilot cues into control in tasks in which extensive experimental data is available [20].

In terms of the piloting tasks to be addressed in this study, the structural pilot modeling approach, cast in a classical, sequential-loop closure format, appears to be the most attractive and useful. This model allows assessment of pilot control behavior in discrete tasks as

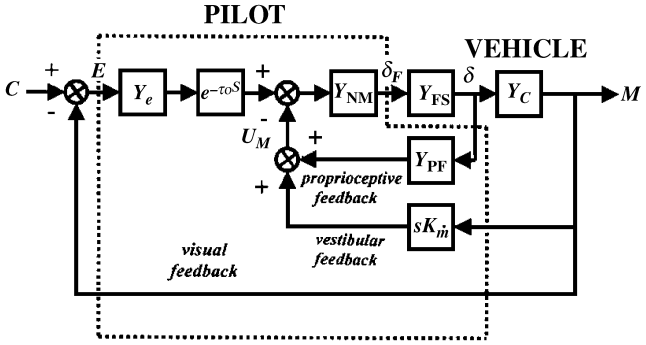

Fig. 1 A structural model of the human pilot in a single-axis task.

well as in tasks involving stochastic environments and is attractive for a number of reasons:

1) It can be viewed in terms of classical flight control contexts.

2) It can provide explicit loop structures that can be tailored to specific task requirements.

3) It is applicable to so-called higher levels of skill development such as pursuit and precognitive modes.

4) It exhibits considerable face validity in its structure, which can be readily related to pilot description of control activity.

5) It is amenable to handling qualities predictions using a handling qualities sensitivity function (HQSF) [13]. Examples of the use of such a modeling approach in realistic, multiaxis tasks, including parameter selection, can be found in [21,22]. A diagram for the structural pilot model for the innermost loop of a multiloop control task is shown in Fig. 1. Here, M could represent vehicle pitch attitude, with C representing a commanded pitch attitude, possibly being generated by an outer-loop position control task as might occur with a hovering rotorcraft. Although the possibility of vestibular feedback is noted in Fig. 1, it will not be used in the analyses and computer simulation to follow. The use and interpretation of this vestibular feedback with the structural model is demonstrated in [23].

The HQSF mentioned previously is defined for each control loop involving the structural pilot model as

$$\text{HQSF} = \frac{1}{|Y_e|}\left|\frac{U_M}{C}\right| \tag{1}$$

where, in most applications, $Y_e = K_e$, a simple gain. Bounds have been established that allow prediction of handling qualities levels for a particular vehicle and task based upon a plot of the HQSF vs. frequency [13,21].

III. Ship Motion

The methodology described in this section is taken directly from the research reported in [11]. This methodology can be used to create power spectral densities (PSDs) of heave, pitch, and roll motion of a monohull ship given relatively simply descriptions of ship size, geometry, speed, and heading, as well as parameters describing sea state. The PSDs of ship motion are given by

$$\Phi_{\text{mm}}(\omega) = |H_m(j\omega)|^2 S(\omega) \tag{2}$$

where

$\Phi_{\text{mm}}(\omega)$ = PSD for the motion variable m (heave, pitch or roll)
$H_m(j\omega)$ = frequency response[†] of the motion variable m
$S(\omega)$ = PSD of the wave motion

The resulting expressions for the motion PSDs are complex algebraic functions of the ship geometry, sea state, etc., and are not amenable to spectrum factorization. Thus, one cannot create the motion time histories by exciting linear shaping filters with white noise. Instead, based upon the work of [11], two functions were created to calculate the PSDs and associated time histories. The function calls are defined as *shiplong* for heave and pitch and *shiplat* for roll. The longitudinal and lateral ship motions are decoupled in this approach.

A. Function Shiplong

The argument list for this function is shiplong (B_0, C_b, F_n, L, T, β, H_S, T_Z). This function is used for finding the PSDs of longitudinal (heave and pitch) ship motion. If β is an odd, integral multiple of $\pi/2$, the predicted pitching motion will be negligible. The input quantities for shiplong are fairly self-explanatory. The block coefficient C_b is simply $C_b = B/B_0$. With $\beta = \pi$ rad, the waves are moving in a direction opposite the course of the ship. T_Z is converted to T_S in shiplong.

The outputs of shiplong are the root mean square (rms) values of heave and pitch, and the amplitudes and frequencies of two sums of n sine waves to be used as the pitch and heave motion time histories. Here $n = 4$. The amplitudes and frequencies of these sinusoids are obtained by considering the integral over frequency of the PSD obtained from shiplong and selecting the frequencies and amplitudes of the sum of sinusoids to approximate this integrated PSD function. This technique has been used in the past in creating sums of sinusoids with PSDs approximating that of stochastic inputs, for example, [24]. A sum of sinusoids is then selected exhibiting a PSD closely approximating that calculated from [11] calculations. Note that information about the relative phasing of pitch and heave motion time histories is lost with this approach.

B. Function Shiplat

The argument list for this function is shiplat (T_N, T, GM_T, B_0, L, β, F_n, μ, H_S, T_Z). This function is used for finding the PSDs of lateral (roll) ship motion. This function treats the ship's submerged hull as a parallelepiped or a wedge. If β is an integral multiple of π, the predicted rolling motion will be negligible. As with shiplong, most of the input parameters for shiplat are self-explanatory. The roll mode time constant T_N for the ship must be estimated. This parameter is essentially the inverse of the period of the roll periodic convergence that would ensue if the ship were disturbed in roll in a calm sea. T_N can be estimated given the ship's moment of inertia about the longitudinal axis, its displacement, and its transverse metacentric height. Viewing the ship from aft, rolled through some small angle ϕ, GM_T describes the distance between two points. The first point is the ship's center of gravity and the second point is the intersection of two lines, one drawn vertically through the center of buoyancy and the second the projection of the hull's plane of symmetry. For small roll angles, this measure is a constant. The ship's velocity enters through the Froude number, defined as

$$F_n = V/\sqrt{gL} \tag{3}$$

The percentage critical damping μ artificially increases the roll damping in the calculations. A value of 40% was used in [11]. The wave zero up-crossing period T_Z is defined as the average time between successive crossings of the mean water level in an upward direction. This parameter is converted to T_S in shiplat.

The outputs of the function shiplat are the rms value of roll and the amplitudes and frequencies of a sum of n sine waves to be used as the roll-motion time histories. Here again, $n = 4$. Table 1, taken from [11], shows the range of H_S and T_Z values that can be encountered in ocean travel. The underlined row and column indicate a pair of values to be used in the example of Sec. V. The quality of the motion prediction scheme used here was compared with experimental results in [11]. One of the ships used in [11] will be used in this study (see Sec. V.A).

IV. Atmospheric Turbulence

The environment in which rotorcraft are required to operate can amplify the importance of atmospheric disturbances in regard to task performance and vehicle handling qualities. This is especially true in flight operations near ships where boxlike structures with sharp

[†]See [11] for a description.

Table 1 Range of H_S and T_Z values (from [11], magnitude of entry indicates relative frequency of occurrence)

T_Z, s	H_S, m											
	1	2	3	4	5	6	7	8	9	10	11	12
1	0	0	0	0	0	0	0	0	0	0	0	0
2	0	0	0	0	0	0	0	0	0	0	0	0
3	0	0	0	0	0	0	0	0	0	0	0	0
4	0	0	0	0	0	0	0	0	0	0	0	0
5	73	5	0	0	0	0	0	0	0	0	0	0
6	1416	356	62	12	2	0.8	0	0	0	0	0	0
7	4594	3299	1084	318	89	20	4.2	0.8	0.2	0	0	0
8	4937	8001	4428	1898	721	203.2	51	10.8	1.6	0.3	0.1	0
9	2590	8022	6920	4126	2039	716.8	217.8	55.2	10	1.7	0.6	0.2
10	839	4393	5566	4440	2772	1186	426	124.8	25.6	5	1.8	0.7

edges and highly turbulent, recirculating flows are common [2]. Any analytical approach to the problem of rotorcraft handling qualities in turbulence requires a realistic but tractable model of the disturbance in question.

Most studies involving fixed-wing aircraft can employ Taylor's hypothesis [25] wherein a frozen turbulence field is employed. The aircraft, with a velocity considerably larger than the rms turbulence velocities at any point, moves through the field. The three mutually perpendicular turbulence velocities can be one-, two-, or three-dimensional functions of spatial displacement from the origin of the frozen field. The legitimacy of the frozen-field hypothesis becomes considerably more tenuous for rotorcraft, especially at low speed. A method for addressing these limitations was discussed in [26], where a simplified approach to modeling the aerodynamic effects of turbulence on rotorcraft was presented.

Analytical and experimental studies summarized in [8,27] and presented in detail in [28] provide an accurate model of turbulence effects on a hovering rotorcraft by determining the control inputs that could be inserted in parallel with those of the pilot so as to produce vehicle responses equivalent to those of a turbulence field. The experiments of [8,27,28] involved a UH-60 rotorcraft hovering on the leeward side of a large, cubelike hangar. The results of these studies were a set of transfer functions, parameterized by main-rotor diameter, turbulence intensity, and mean wind speed. When excited by unity covariance white noise, the transfer functions would produce control inputs (longitudinal cyclic, lateral cyclic, and main- and tail-rotor collective) that would create forces and moments on the vehicle equivalent to the turbulence field in which the rotorcraft was hovering. An example of one such transfer function is shown next.

$$\left.\frac{\delta_c}{\text{wn}}(s)\right|_{\text{swashplateUH-60}} = 0.1486(\sigma_w)^{-0.7069} \times \sqrt{\frac{3\sigma_w^2 V_r}{\pi r}}\left\{\frac{s + 33.91(V_r/R_m)}{[s + 1.46(V_r/R_m)][s + 9.45(V_r/R_m)]}\right\} \text{ deg} \quad (4)$$

Reference [9] provides an approximate technique for scaling transfer functions such as that in Eq. (4) so as to be applicable to rotorcraft other than the UH-60.

It is obvious that the method of handling atmospheric disturbances just outlined cannot capture the detailed flow characteristics that can be obtained with CFD techniques in which the geometry of the particular ship in question is modeled. However, the simplicity of the technique just described as well as its ability to produce results similar to those obtained with a blade element approach as reported in [28] strongly suggest its use here.

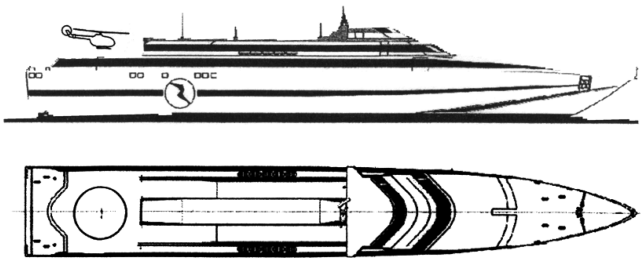

Fig. 2 A fast ferry TMV 114.

V. An Example

A. Ship Model

The ship model chosen for study is taken from [11] and referred to their as a *fast ferry* with designation TMV 114. Figure 2 shows the ship. This ship is clearly a nonaviation vessel. It has been chosen here simply because the information required to generate ship motion was available from [11] and the resulting motion associated with this vessel can be considerable. In addition, experimental data was available with which to compare the modeling results, as was done in [11]. The landing pad suggested in Fig. 2 is an artifact here. The TMV 114 has the following particulars: $L = 96$ m, $B_0 = 13.8$ m, $T = 2.5$ m, $C_b = 0.53$, $GM_T = 4.19$ m, and $T_N = 6.3$ s. The ship speed will be selected as 20 kn, which yields $F_n = 0.34$. The center of gravity of the ship was assumed to be amid ship, along the ship centerline, approximately 3.3 m above the waterline. Although the vessel is equipped with submerged, extensible foils, they were not modeled in this study.

B. Rotorcraft Model

The rotorcraft selected for study is the BO-105 with aerodynamic data taken from [29]. The vehicle is shown in Fig. 3. The main-rotor diameter is 9.82 m. Aerodynamic data for a variety of velocities are available from [29]. The data for $U_0 = 10$ kts was chosen. The reason for this nonzero trim airspeed will be explained in Sec. V.E.

The basic vehicle dynamics were augmented in the pitch, roll, and yaw axes through the introduction of the stability and command augmentation system (SCAS). For the pitch and roll axes, the SCAS designs were rate-command, attitude hold (RCAH) systems with bandwidths of approximately 3.0 rad/s[‡]. For the yaw axis, the SCAS was a rate-command (RC) design, with a bandwidth of approximately 4.4 rad/s. No augmentation of the heave axis was implemented. Identical actuators were modeled with transfer functions given by

$$G_{\text{ACT}} = \frac{30^2}{s^2 + 2(0.7)30s + 30^2} \quad (5)$$

Details of the vehicle model, SCAS designs, and assumed cockpit force/feel systems are given in the Appendix. As in previous applications of the structural pilot model, control sensitivity issues were not addressed in the SCAS designs,that is, in the RCAH and RC systems. This sensitivity has no impact upon the simulated vehicle responses or the handling qualities analysis using the HQSF [13].

[‡]Bandwidths were based upon the frequency at which a 135-deg phase lag occurred in the closed loop in the rate-command system transfer functions.

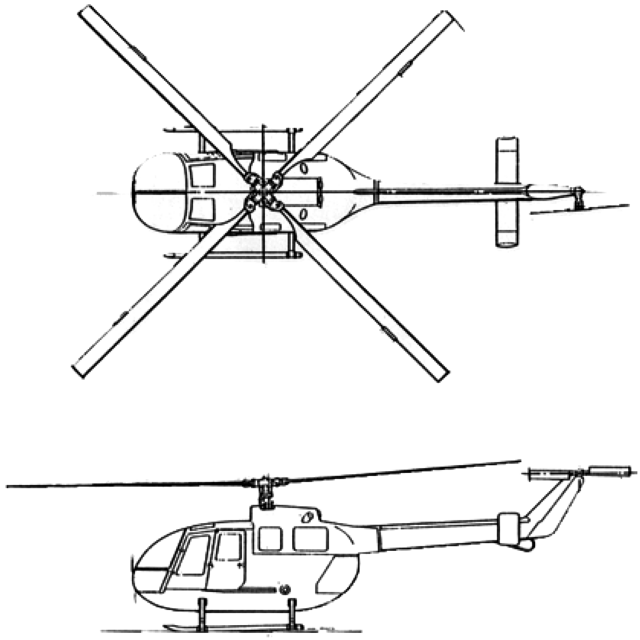

Fig. 3 The BO-105 rotorcraft.

C. Turbulence Model and Scaling

The following turbulence transfer functions were obtained from the NASA Ames Research Center for the UH-60 rotorcraft as derived from the flight tests described in [8,28]. The control inputs are in terms of swashplate deflections on the UH-60. All units are in the SI system.

$$\left.\frac{\delta_A}{\text{wn}}\right|_{\text{swashplateUH-60}} = 0.837\sigma_w^{-0.6265}\sqrt{\frac{\sigma_w^2 V_r}{\pi r}}\left[\frac{1}{s+(2V_r/R_m)}\right] \text{ deg} \tag{6}$$

$$\left.\frac{\delta_B}{\text{wn}}\right|_{\text{swashplateUH-60}} = 1.702\sigma_w^{-0.6265}\sqrt{\frac{\sigma_w^2 V_r}{\pi r}}\left[\frac{1}{s+(2V_r/R_m)}\right] \text{ deg} \tag{7}$$

$$\left.\frac{\delta_C}{\text{wn}}(s)\right|_{\text{swashplateUH-60}} = 0.1486(\sigma_w)^{-0.7069} \times \sqrt{\frac{3\sigma_w^2 V_r}{\pi r}}\left\{\frac{s+33.91(V_r/R_m)}{[s+1.46(V_r/R_m)][s+9.45(V_r/R_m)]}\right\} \text{ deg} \tag{8}$$

$$\left.\frac{\delta_P}{\text{wn}}\right|_{\text{swashplateUH-60}} = 1.573\sigma_w^{-0.6493}\sqrt{\frac{\sigma_w^2 V_r}{\pi r}}\left[\frac{1}{s+(V_r/R_m)}\right] \text{ deg} \tag{9}$$

where δ_P refers to tail-rotor collective input.

The scaling procedure of Eqs. (6–9) was applied to the transfer functions of Eqs. (6) to adapt them to the BO-105 vehicle. For example, for the BO-105, Eq. (6) takes the form

$$\left.\frac{\delta_A}{\text{wn}}\right|_{\text{swashplateBO-105}} = 0.17\sigma_w^{+0.375}V_r^{0.5}\left(\frac{s+0.048V_r}{(s+0.244V_r)(s+0.08V_r)}\right) \text{ deg} \tag{10}$$

To serve as an input to the rotorcraft model, the swashplate deflection needs to be converted into equivalent displacement of the cockpit controller at the pilot's hand. For Eq. (10), [29] indicates this conversion is $K_{\delta_A} = 0.7846$ cm/ deg.

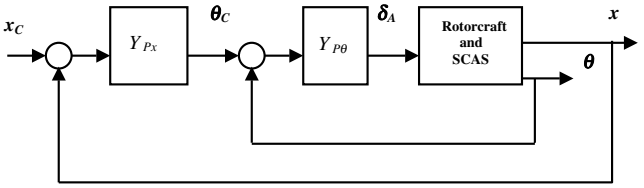

Fig. 4 Sequential-loop closure, compensatory pilot control strategy.

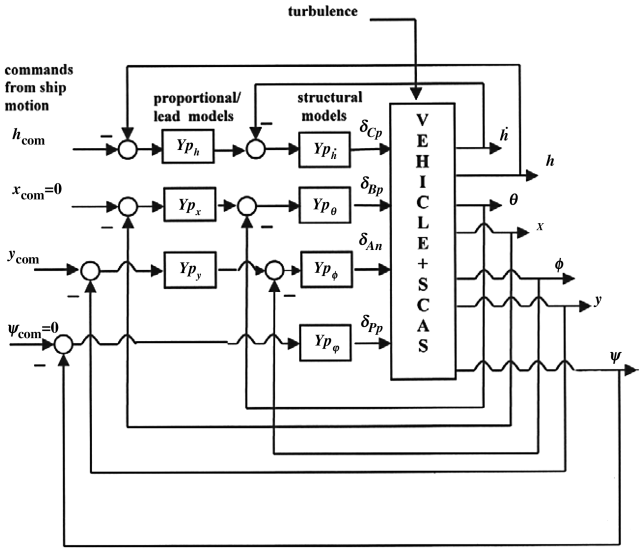

Fig. 5 Complete pilot/vehicle system.

D. Pilot Models: Compensatory Strategies

Figure 4 shows the sequential, compensatory pilot control strategy that will be employed in each control loop. Here, longitudinal control is shown.

Task-dependent handling qualities will be ascertained in a manner similar to that proposed in [21]. The parameters of the structural pilot models for the inner attitude and vertical translation rate loops were selected using the technique discussed in [30]. The nominal crossover frequencies were selected as 1.5 rad/s in each loop. The outer-loop pilot transfer functions, for example, Yp_x in Fig. 4, were selected to provide K/s-like frequency characteristics at the desired outer-loop crossover frequencies. These latter crossover frequencies were selected as one-third of those of the nominal inner loops, that is, 0.5 rad/s. Figure 5 provides a diagram of the entire pilot/vehicle feedback system. Details of the pilot models are given in the Appendix.

With the multiloop pilot/vehicle system of Fig. 5, calculation of the HQSF for each loop is still accomplished with Eq. (1), however, all remaining loops remain closed. This allows the HQSF calculated for any control loop to reflect the complete closed-loop system. Reference [21] indicates that this approach allows the HQSF indicating the poorest handling qualities to reflect the handling qualities level for the entire multiloop piloting task at hand.

E. Environment and Piloting Task Descriptions

The ship of Fig. 2 will be assumed to be traveling at 20 kn (speed relative to a quiescent sea and atmosphere). The following parameter selections were made: $\beta = 135$ deg, $H_S = 2$ m, and $T_Z = 10$ s. The latter two selections correspond to the entry in the tenth row and third column of Table 1. Equations describing the resulting landing pad motions are given in the Appendix.

For the turbulence models, $V_r = 5.144$ m/s (10 kn: approximately 50% of the velocity of the ship relative to a quiescent atmosphere) and $\sigma_w = 1.03$ m/s (2 kn: approximately 10% of the

Table 2 Task performance criteria

Performance	Long.	Lateral	Vertical	Heading
Desired	±1.5 m	±2 m	±3 m	±5 deg
Adequate	±2 m	±3 m	±4 m	±10 deg

velocity of the ship relative to a quiescent atmosphere). There obviously exists a range of turbulence parameter values that could be selected. The values chosen here are not arbitrary, but have been selected based upon experimental results reported in [2,27,28]. In [27,28] mean wind speed (at the hangar roof), mean wind speed at the rotorcraft location, and the rms turbulence have an approximate ratio of 1:(0.58):(0.13). In [2], experimental data for a model of an amphibious assault ship suggests an approximate ratio of 1:(0.4):(0.05). Note that here V_r subsumes the effects of any mean wind speed that may exist above the 20 kn figure cited in Sec. V.A. A V_r of 10 kn explains the choice of a 10 kn trim airspeed in Sec. V.B. No steady crosswinds were assumed. A complete list of the turbulence transfer functions is given in the Appendix.

The piloting task consists of maintaining the vehicle in hover at a nominal height of 5 m over the ship's landing pad. The vehicle is to remain within a rectangular parallelepiped that translates with the pad's vertical and lateral motion and to maintain heading relative to the longitudinal axis of the ship. The dimensions of the parallelepiped define desired and adequate performance and are given in Table 2 along with the criteria on vehicle heading. The author realizes that this particular task is not representative of operational shipboard recovery procedures. In these procedures, pilots often hover at a prescribed height above the deck and wait for a quiescent period in ship motion. When such a period occurs, a landing is made. The task here was chosen primarily as a handling qualities evaluation task for the purposes of this study.

F. Computer Simulation Results

Figures 6–8 show the PSDs of the ship pitch, heave, and roll motions, and Figs. 9–11 show the resulting sum of sinusoids time histories. Note that the pitch, heave, and roll motions were transformed into lateral and vertical motions of the landing pad (longitudinal motion over and above the 20 kn ship velocity was neglected). Figure 12 shows the resulting landing pad motions. Figure 13 shows a sample of the control inputs that created the equivalent atmospheric turbulence. Following the convention of [29], these inputs are given in terms of equivalent motion of the controllers in the cockpit at the pilot's hands and feet.

Figures 14–18 show the pilot/vehicle performance in each axis for this task. The ordinates of each figure are scaled such that the maximum values correspond to the limits for desired performance

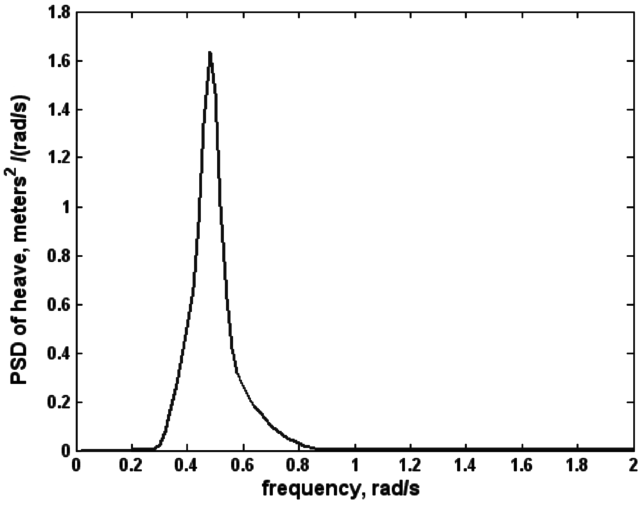

Fig. 6 PSD of ship heave motion.

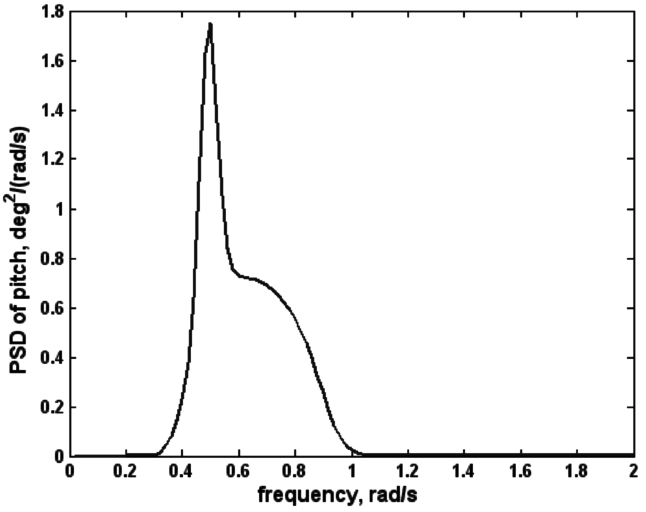

Fig. 7 PSD of ship pitch motion.

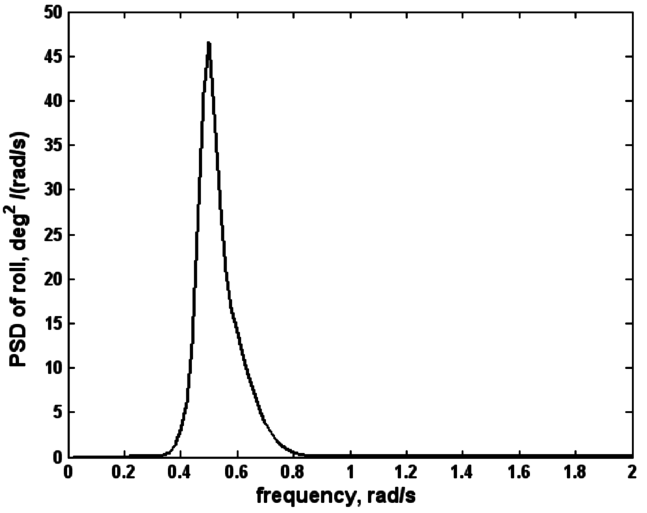

Fig. 8 PSD of ship roll motion.

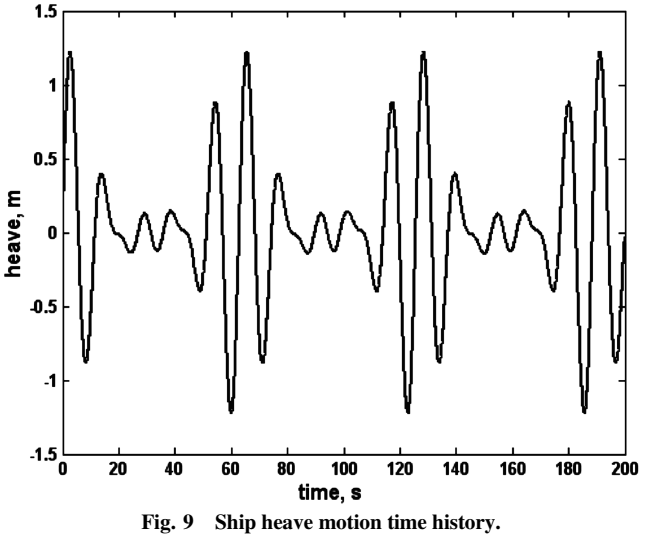

Fig. 9 Ship heave motion time history.

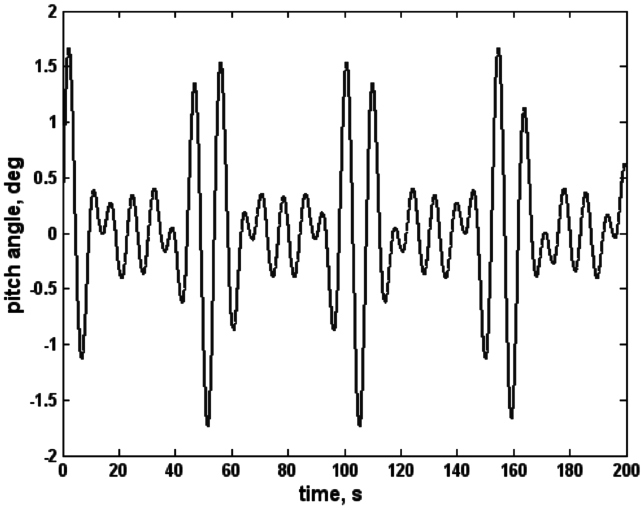

Fig. 10 Ship pitch-motion time history.

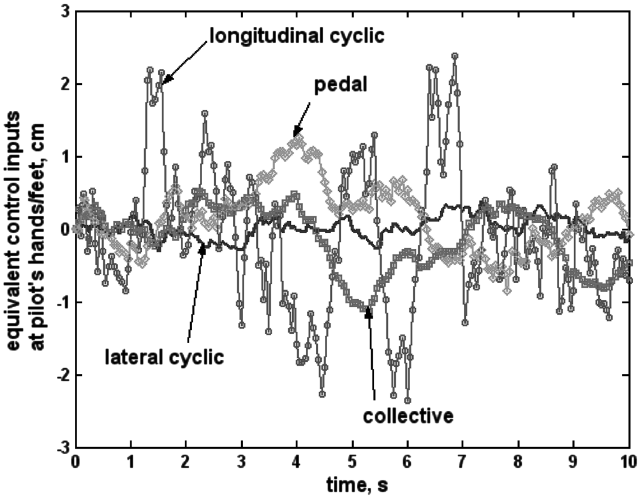

Fig. 13 Control inputs for turbulence modeling.

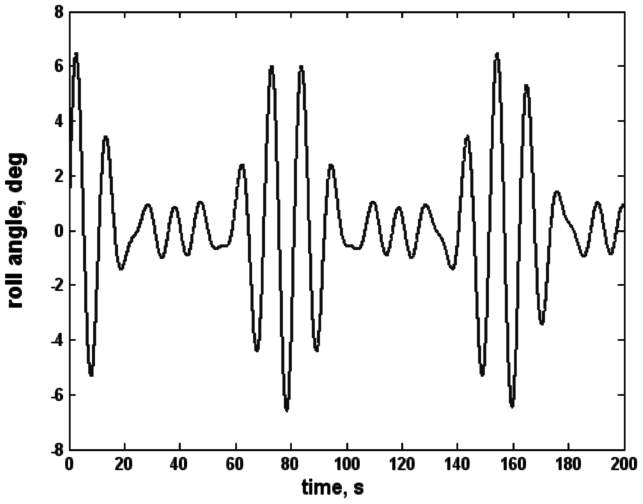

Fig. 11 Ship roll-motion time history.

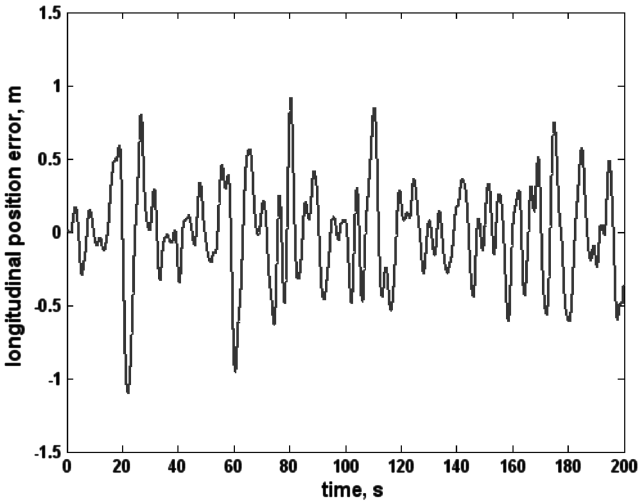

Fig. 14 Longitudinal position error.

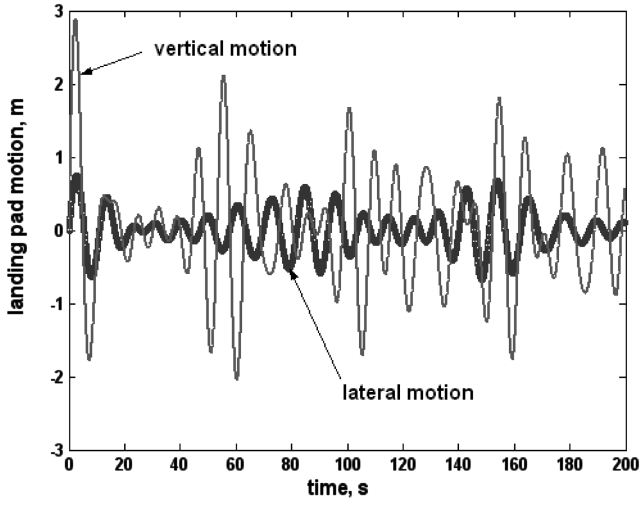

Fig. 12 Ship landing pad motion.

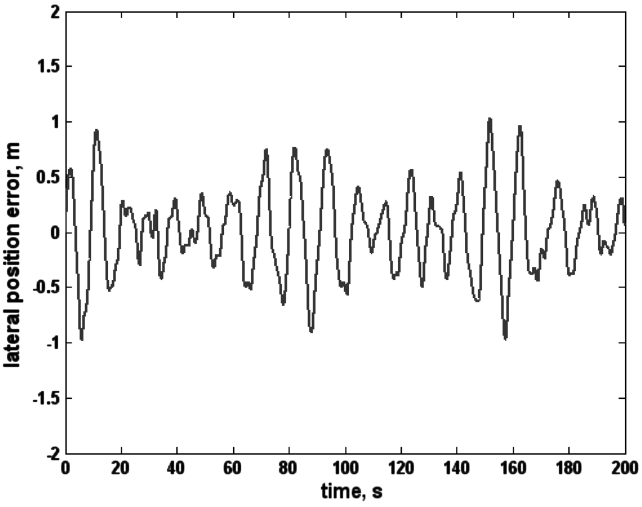

Fig. 15 Lateral position error.

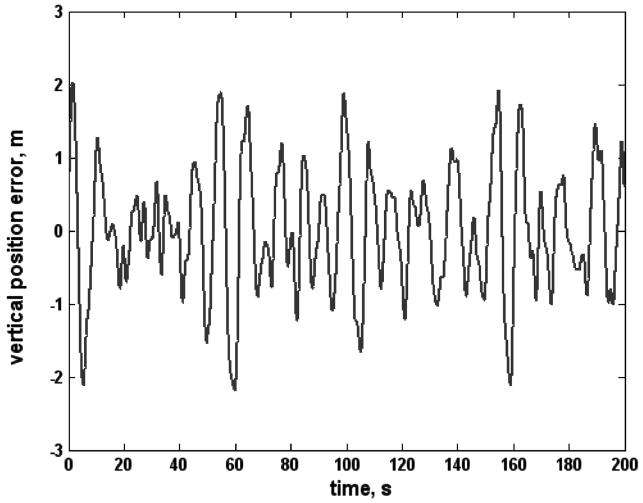

Fig. 16 Vertical position error.

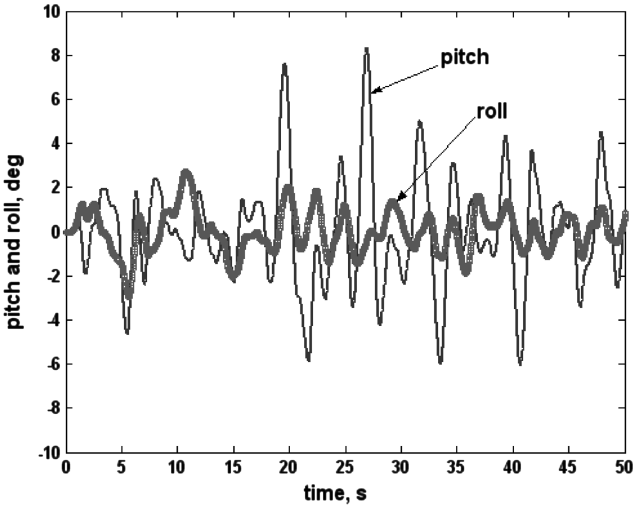

Fig. 18 Rotorcraft pitch and roll attitude.

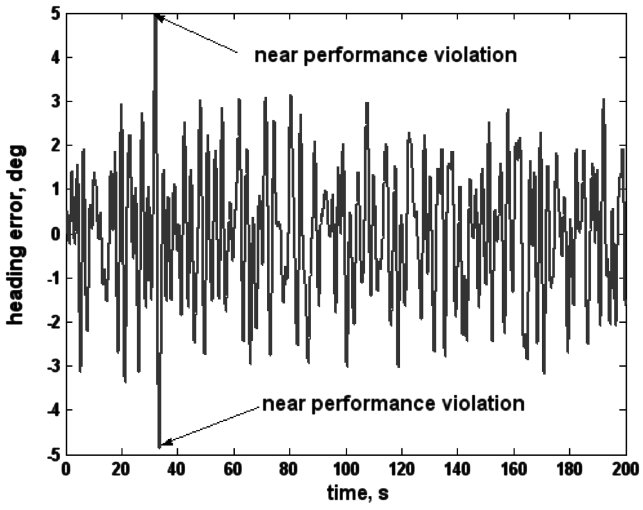

Fig. 17 Rotorcraft heading error.

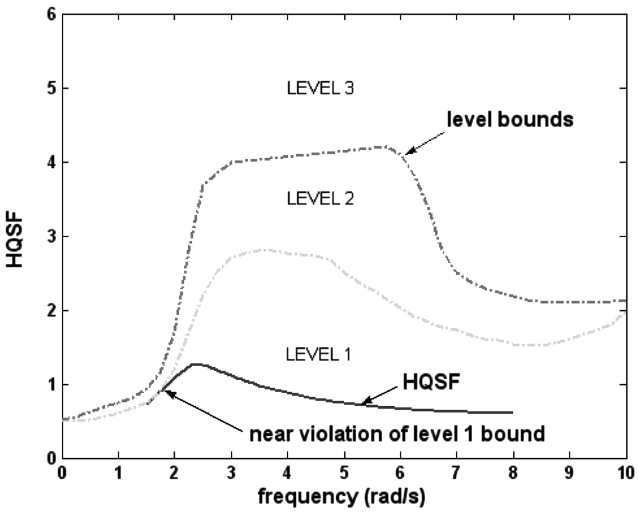

Fig. 19 HQSF for heading loop.

given in Table 2. To obtain satisfactory performance in heading, the structural model crossover frequency in the heading loop had to be increased from 1.5 to 2.0 rad/s. Two very brief excursions near the ±5 deg limit occur in heading error with this larger crossover frequency. As the figures indicate, desired performance is obtained in all axes. However, a comparison of the pad motions that serve as commands to the pilot/vehicle system (Fig. 12), with the resulting tracking errors (Figs. 14–16), clearly indicates that the errors are of the same order of magnitude as the commands. This is not surprising given the fact that the ship motion PSDs of Figs. 6–8 contain most of their power at a frequency very near the crossover frequencies of the outer control loops closed by the pilot (0.5 rad/s). Runs made excluding turbulence do not appreciably alter this result. Turbulence does have a pronounced effect upon performance in the yaw axis. Without atmospheric disturbances, heading performance is significantly improved, with maximum heading deviations reaching only 20% of those resulting when turbulence was included.

An examination of the task-dependent HQSF[§] indicates that the heading loop came closest to a violation of the leve1 1 boundaries also. This HQSF is shown in Fig. 19. The final conclusion is that the task-dependent handling qualities would be borderline level 1 and control of the yaw axis would create the highest pilot workload. This workload is predicted to be attributable to the turbulence environment.

[§]Task dependency is accommodated by the technique discussed in [21].

G. Discussion

The analyses and computer simulation described in the previous sections are not offered as a replacement for more detailed and complex representations of rotorcraft operation near ships. Rather, the author suggests that the proposed approach may allow the control system or handling qualities engineer to establish rotorcraft control system requirements using a relatively simple and tractable methodology. The more sophisticated and computationally intensive modeling approaches such as those discussed in [6] can be reserved for evaluation of final designs. The particular ship and rotorcraft selected for study were chosen entirely on the basis of data availability and the fact that no proprietary or other limitations would limit publication. As was mentioned in Sec. V.E, selection of the turbulence parameters was based upon limited experimental results. In applying the proposed methodology, a range of turbulence parameters could be incorporated in the simulation. Validation of the methodology through comparison with the more sophisticated modeling approaches just referenced is warranted.

Finally, as was mentioned in Sec. V.E, the task chosen for simulation and analysis is somewhat artificial in that the "deck chasing" that occurs is not representative of operational procedures. An interesting extension of this work would include a more realistic task. As an example, Fig. 12 indicates time segments in which there is relatively little ship motion. Increasing the number of sinusoids used to describe the ship motion power spectra may emphasize these lull

periods. The pilot model could then be used to simulate an attempted touchdown in these periods.

VI. Conclusion

Based upon the research summarized herein, the following conclusions can be drawn:

1) A simplified technique for evaluating flight control system designs for piloted rotorcraft operations near ships is feasible.

2) An approximate technique for generating ship motion and turbulence can be used in the analysis and simulation.

3) Used in conjunction with an established pilot modeling procedure, estimates of handling qualities levels can be made for flight tasks conducted near ships. These estimates can accommodate task demands.

4) A comparison of the results of this simplified approach with those of more detailed modeling procedures should be undertaken. This is particularly true for the turbulence modeling where the scaling procedure has yet to be validated through comparison with experiment.

Appendix

Vehicle Model: BO-105 Rotorcraft

$$\{\dot{x}(t)\} = [A]\{x(t)\} + [B]\{\delta(t)\}$$

where

$$\{x(t)\} = [u(t), w(t), q(t), \theta(t), v(t), p(t), r(t), \phi(t), \varphi(t)]^T$$

$$\{\delta(t)\} = [\delta_C(t), \delta_B(t), \delta_A(t), \delta_P(t)]^T$$

$$[A] = \begin{bmatrix} -0.0196 & 0148 & 0.5201 & -9.81 & 0 & -0.2907 & -0.0245 & 0 & 0 \\ -0.1320 & -0.3768 & 5.19 & 0 & 0.0025 & -0.0505 & 0.4668 & 0 & 0 \\ 0.0593 & -0.0012 & -3.4105 & 0 & -.0158 & -0.86 & 0.0494 & 0 & 0 \\ 0 & 0 & 1 & 0 & 0 & 0 & 0 & 0 & 0 \\ 0.0037 & -0.0045 & -0.1595 & 0 & -0.1259 & -0.6369 & -5.019 & 9.81 & 0 \\ -0.0202 & -0.0111 & 2.3180 & 0 & -0.2290 & -9.4386 & 0.0537 & 0 & 0 \\ -0.0233 & 0.0079 & -0.601 & 0 & 0.0474 & 0.1119 & -0.4741 & 0 & 0 \\ 0 & 0 & 0 & 0 & 0 & 1 & 0 & 0 & 0 \\ 0 & 0 & 0 & 0 & 0 & 0 & 1 & 0 & 0 \end{bmatrix}$$

$$[B] = \begin{bmatrix} 0.0388 & 0.0957 & -0.0031 & -0.0144 \\ -1.1544 & 0.0364 & 0.0039 & 0.0024 \\ 0.0004 & -0.3844 & 0.0674 & 0.0248 \\ 0 & 0 & 0 & 0 \\ -0.0116 & 0.0011 & 0.0986 & -0.1919 \\ -0.0698 & 0.1739 & 1.0450 & -0.3902 \\ 0.2203 & 0.0080 & 0.0153 & 0.5353 \\ 0 & 0 & 0 & 0 \\ 0 & 0 & 0 & 0 \end{bmatrix}$$

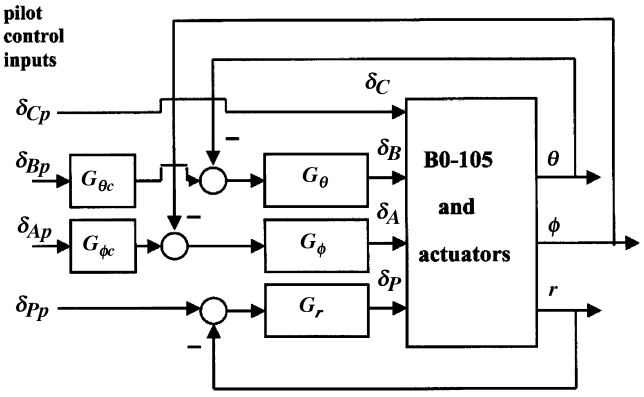

Fig. A.1 SCAS block diagram.

Stability and Command Augmentation Systems

Transfer functions are shown in Fig. A.1.

$$G_{\theta c} = \frac{0.848}{s}; \qquad G_{\phi c} = \frac{0.95}{s}$$

$$G_\theta = \frac{-11(s+0.4)^2(s+3)}{s^2(0.05s+1)}$$

$$G_\phi = \frac{4.18(s+0.4)^2(s+8)}{s^2(0.05s+1)}; \qquad G_r = \frac{10(s+0.7)}{s}$$

Cockpit Force/Feel System Dynamics

Lateral cyclic, longitudinal cyclic, and pedals

$$Y_{\mathrm{FS}}(s) = \frac{25^2}{s^2 + 2(0.7)25s + 25^2}$$

Collective

$$Y_{\mathrm{FS}}(s) = \frac{1 \cdot 10^3}{(s+10)(s+100)}$$

Because of the manner in which the structural model is formulated, the particular units on the Y_{FS} functions are of no consequence.

Pilot Models

Structural Model Elements for Inner Loops

Transfer functions can be found in Fig. 1.

All loops ($\tau_0 = 0.2$ s)

$$Y_{\mathrm{NM}} = \frac{10^2}{s^2 + 2(.707)10s + 10^2}$$

θ, ϕ, r loops

$$Y_{\mathrm{PF}} = 1.65;$$
$$Y_{e\theta} = 4.0; \qquad Y_{e\phi} = 3.45; \qquad Y_{e_r} = 3.83;$$
$$K_{\dot{m}} = 0$$

h-dot loop

$$Y_{\mathrm{PF}} = 2.05; \qquad Y_{e\dot{h}} = 3.95; \qquad K_{\dot{m}} = 0$$

Pilot Model Elements for Outer Loops

x, y loop

$$Yp_x = -0.0531\frac{(s+0.1)}{0.5s+1}; \qquad Yp_y = 0.0545\frac{(s+0.1)}{0.5s+1}$$

Transfer functions can be found in Fig. 5.

h loop

$$Yp_h = -0.494$$

For the ψ loop, no outer φ loop is necessary.

Turbulence Transfer Functions

These transfer functions are scaled for the BO-105 rotorcraft and expressed in terms of equivalent cockpit control motion at the pilot's hands and feet.

$$\left.\frac{\delta_A}{\mathrm{wn}}\right|_{\mathrm{BO\text{-}105}} = \frac{0.17\sigma_w^{+0.3735}V_r^{0.5}(s+0.048V_r)}{(s^2+0.324V_rs+0.0195V_r^2)} \text{ deg } \cdot 0.785 \text{ cm/ deg}$$

$$\left.\frac{\delta_B}{\mathrm{wn}}\right|_{\mathrm{BO\text{-}105}} = \frac{0.345\sigma_w^{+0.3735}V_r^{0.5}(s+0.048V_r)}{(s^2+0.324V_rs+0.0195V_r^2)} \text{ deg } \cdot 3.08 \text{ cm/ deg}$$

$$\left.\frac{\delta_C}{\mathrm{wn}}\right|_{\mathrm{BO\text{-}105}} = \frac{0.0537\sigma_w^{+0.2931}V_r^{0.5}(s^2+4.2V_rs+0.2V_r^2)}{(s^3+1.42V_rs^2+0.314V_r^2s+0.0166V_r^3)} \text{ deg } \cdot \times 1.63 \text{ cm/ deg}$$

$$\left.\frac{\delta_P}{\mathrm{wn}}\right|_{\mathrm{BO\text{-}105}} = \frac{0.28\sigma_w^{+0.3057}V_r^{0.5}}{(s+0.122V_r)} \text{ deg } \cdot 0.689 \text{ cm/ deg}$$

Ship Motion: Fast Ferry TMV 114

$T_Z = 10$ s and $H_S = 2$ m.

$$h_S(t) = [0.2172\sin(0.4t) + 0.4714\sin(0.5t) + 0.3592\sin(0.6t) + 0.2227\sin(0.7t)] \text{ m}$$

$$\theta_S(t) = [0.005\sin(0.46t) + 0.00964\sin(0.58t) + 0.00725\sin(0.7t) + 0.00845\sin(0.82t)] \text{ rad}$$

$$\phi_S(t) = [0.021\sin(0.46t) + 0.0431\sin(0.54t) + 0.290\sin(0.62t) + 0.022\sin(0.67t)] \text{ rad}$$

Motion for Landing Pad Vertical Motion h_P and Lateral Motion y_P

$$h_P = 57.11\sin(\theta_S t) + 13.2[\sin(0.5\phi_S t)]^2 + h_S(t) \text{ m};$$
$$y_P = 6.6\sin(\phi_S t) \text{ m}$$

Acknowledgement

The research reported herein was supported by a Phase II SBIR award, contract no. N68335-05-C-0054. The project is entitled "Pilot Behavioral Modeling for Flight Operations Near Ships," performed for the Naval Air Warfare Center (Aircraft Division), Patuxent River, MD, and is under the direction of Robert Heffley Engineering, Los Altos, CA.

References

[1] Newman, J. N., "The Theory of Ship Motions," *Advances in Applied Mechanics*, Vol. 18, 1978, pp. 221–283.

[2] Healy, J. V., "Establishing a Database for Flight in the Wakes of Structures," *Journal of Aircraft*, Vol. 29, No. 4, 1992, pp. 559–564.

[3] Rhoades, M. M., and Healy, J. V., "Flight Deck Aerodynamics of a Nonaviation Ship," *Journal of Aircraft*, Vol. 29, No. 4, 1992, pp. 619–626.

[4] Bogstad, M. C., Habashi, W. G., Akel, I., Ait-Ali-Yahia, D., Giannias, N., and Longo, V., "Computational-Fluid-Dynamics Based Advanced Ship-Airwake Database for Helicopter Flight Simulators," *Journal of Aircraft*, Vol. 39, No. 5, 2002, pp. 830–838.

[5] Wakefield, N. H., Newman, S. J., and Wilson, P. A., "Helicopter Flight Around a Ship's Superstructure," *Journal of Aerospace Engineering*, Vol. 216, Part G, 2002, pp. 13–28.

[6] Lee, D., Horn, J. F., Sezer-Uzol, N., Horn, J. F, and Long, L. N., "Simulation of Helicopter Shipboard Launch and Recovery with Time-Accurate Airwakes," *Journal of Aircraft*, Vol. 42, No. 2, 2005, pp. 448–461.

[7] Lee, D., and Horn, J. F., "Analysis of Pilot Workload in the Helicopter/Ship Dynamic Interface Using Time-Accurate and Stochastic Ship Airwake Models," AIAA Paper 2005-5360, 2005.

[8] Lusardi, J. A. Tischler, M B., Blanken, C. L. and Labows, S. J., "Empirically Derived Helicopter Response Model and Control System Requirements for Flight in Turbulence," *Journal of the American Helicopter Society*, Vol. 49, No. 3, 2004, pp. 340–349.

[9] Hess, R. A., "A Simplified and Approximate Technique for Scaling Rotorcraft Control Inputs for Turbulence Modeling," *Journal of the American Helicopter Society*, Vol. 49, No. 3, 2004, pp. 361–366.

[10] Geyer, W. P., Smith, E. C., and Keller, J. A., "Aeroelastic Analysis of Transient Blade Dynamics During Shipboard Engage/Disengage Operations," *Journal of Aircraft*, Vol. 35, No. 3, 1998, p. 453.

[11] Jensen, J. J., Mansour, A. E., and Olsen A. S., "Estimation of Ship Motions Using Closed-Form Expressions," *Ocean Engineering*, Vol. 31, No. 1, 2004, pp. 61–85.

[12] McRuer, D. T., and Krendel, E., "Mathematical Models of Human Pilot Behavior," NATRO Advisory Group for Aerospace Research and Development, AGARDograph 188, 1974.

[13] Hess, R. A., "Unified Theory for Aircraft Handling Qualities and Adverse Aircraft-Pilot Coupling," *Journal of Guidance, Control, and Dynamics*, Vol. 20, No. 6, 1997, pp. 1141–1148.

[14] Van Paassen, R., "Biophysics in Aircraft Control: A Model of the Neuromuscular System of the Pilot's Arm," Ph.D. Dissertation, Faculty of Aerospace Engineering, Delft Univ. of Technology, The Netherlands, 1994.

[15] Jex, H. R., "Problems in Modeling Man-Machine Control Behavior in Biodynamic Environments," *Proceedings of the Seventh Annual Conference on Manual Control*, NASA, 1971, pp. 3–14; also, NASA SP-281, June–1971.

[16] Kleinman, D. L., Baron, S., and Levison, W. H., "An Optimal Control Model of Human Response, Part 1," *Automatica: the Journal of IFAC, the International Federation of Automatic Control*, Vol. 6, No. 3, 1970, pp. 357–369.

[17] Davidson, J. D., and Schmidt, D. K., "Modified Optimal Control Pilot Model for Computer-Aided Design and Analysis," NASA TM 4384, NASA Langley Research Center, 1992.

[18] Zeyada, Y., and Hess, R. A., "Human Pilot Cue Utilization with Applications to Simulator Fidelity Assessment," *Journal of Aircraft*, Vol. 37, No. 4, 2000, pp. 588–597.

[19] Kramer, U., "On the Application of Fuzzy Sets to the Analysis of the System-Driver-Vehicle Environment," *Automatica: the Journal of IFAC, the International Federation of Automatic Control*, Vol. 2, No. 1, 1985, pp. 101–107.

[20] Jagacinski, R. J., and Flach, J. M., *Control Theory for Humans–Quantitative Approaches to Modeling Performance*, Erlbaum, Mahwah, NJ, 2003, Chap. 24.

[21] Hess, R. A., Zeyada, Y., and Heffley, R. K., "Modeling and Simulation for Helicopter Task Analysis," *Journal of the American Helicopter Society*, Vol. 47, No. 4, 2002, pp. 243–252.

[22] Zeyada, Y., and Hess, R. A., "Computer-Aided Assessment of Flight Simulator Fidelity," *Journal of Aircraft*, Vol. 40, No. 1, 2003.

[23] Hess, R. A., "Theory for Roll-Ratchet Phenomenon in High Performance Aircraft," *Journal of Guidance, Control, and Dynamics*, Vol. 21, No. 1, 1998, pp. 101–108.

[24] Hess, R. A., "Application of a Model-Based Flight Director Design Technique to a Longitudinal Hover Task," *Journal of Aircraft*, Vol. 14, No. 3, 1977, pp. 265–271.

[25] Houbolt, J. C., "Atmospheric Turbulence," *AIAA Journal*, Vol. 11, No. 4, 1973, pp. 421–437.

[26] Hess, R. A., "Rotorcraft Handling Qualities in Turbulence," *Journal of Guidance, Control, and Dynamics*, Vol. 18, No. 1, 1995, pp. 39–45.

[27] Labows, S., "UH-60 Black Hawk Disturbance Rejection Study for Hover/Low Speed Handling Qualities Criteria and Turbulence Modeling," M.S. Dissertation, Dept. of Aeronautics, Naval Postgraduate School, Monterey, CA, 2000.

[28] Lusardi, J. A., "Control Equivalent Turbulence Inputs Model for the UH-60," Ph.D. Dissertation, Department of Mechanical and Aeronautical Engineering, Univ. of California, Davis, Davis, CA, 2004.

[29] Heffley, R. K., Jewell, W. F., Lehman, J. M, and Van Winkle, R. A., "A Compilation and Analysis of Helicopter Handling Qualities Data, Vol. 1: Data Compilation," NASA CR-3144, March 1979.

[30] Hess, R. A., "Human-in-the-Loop Control," *The Control Handbook*, edited by W. S. Levine, CRC Press, Boca Raton, FL, 1996, Chap. 80.